Control Parameters for Track Continuity of Cyclones Passing over the South-Central Appalachian Mountains

RIEM ROSTOM

Department of Energy and Environmental Systems, North Carolina A&T State University, Greensboro, North Carolina

YUH-LANG LIN

Department of Energy and Environmental Systems, and Department of Physics, North Carolina A&T State University, Greensboro, North Carolina

(Manuscript received 14 July 2014, in final form 20 April 2015)

ABSTRACT

The tracks of all 42 tropical cyclones (TCs) passing over the south-central Appalachians from the east or west during 1850–2011 are found to be continuous. By estimating the basic-flow and vortex Froude numbers, and the basic-flow and vortex Rossby numbers (U/Nh, V_{max}/Nh, U/fL_x, and V_{max}/fR, respectively; where U is the basic-flow speed, V_{max} is the maximum tangential wind speed, N is the buoyancy frequency, h is the mountain height, f is the Coriolis parameter, R is the radius of cyclone center to V_{max}, and L_x is the mountain width), from the hurricane reanalysis data, the lack of track discontinuity is explained by weaker blocking associated with lower mountains. The track discontinuity is found to be mainly controlled by V_{max}/Nh and V_{max}/fR (greater than 1.5 and 4.0, respectively), and less sensitive to U/Nh and U/fL_x, consistent with a previous study. It is hypothesized that stronger blocking associated with weaker near-surface tangential winds of extratropical cyclones tends to make their tracks across the Appalachians discontinuous. This hypothesis is verified by investigating 13 heavy snowstorms with discontinuous tracks during 1950–2003. The present results show that all V_{max}/Nh fall below 1.5 and all V_{max}/fR fall below 4.0. To help understand the dynamics associated with orographic blocking, the 2–5 February 1995 snowstorm is simulated by a numerical model. The simulated results indicate that the upstream V_{max}/Nh and V_{max}/fR are indeed less than 1.5 and 4.0, respectively. Therefore, it is concluded that track discontinuity of a cyclone passing over a mesoscale mountain is mainly controlled by strong orographic blocking as measured by lower vortex Froude number (i.e., V_{max}/Nh) and/or lower vortex Rossby number (i.e., V_{max}/fR).

1. Introduction

Floods that occur during the fall season over the Appalachians in the United States are in most cases the result of enhanced heavy rainfall from hurricanes. This observation is consistent with floods resulting from the passage of typhoons over the Central Mountain Range (CMR) in Taiwan (Lin 2007). Strong orographic lifting is often observed over windward slopes resulting in enhanced rainfall and catastrophic flooding. For example, Hurricane Camille (1969) dumped up to 686 mm of rainfall in one location in 12 h along the slope of the Appalachian Mountains in central Virginia (Schwarz 1970). Similarly, on 16 September 2004 in Macon County, North Carolina, Hurricane Ivan produced a debris flow causing five deaths and two injuries along with the destruction of 16 buildings (Stewart 2005). During the 2004 hurricane season, the total damage from hurricanes was estimated to be $45 billion in the United States (Franklin et al. 2006). Some of those damages were related to flash flooding caused by heavy orographic rainfall. The distribution and location of maximum rainfall associated with tropical cyclones (TCs) that pass over mountains are highly sensitive to the TC tracks [Atallah and Bosart (2003); Atallah et al. (2007); Lin et al. (2005, hereafter L05); Lin (2007)]. Looking at the rainfall maps of storms from the National Climatic Data Center (NCDC), it is clear that different tracks produce different rainfall patterns. To improve

Corresponding author address: Dr. Yuh-Lang Lin, EES/ISET, North Carolina A&T State University, 302H Gibbs Hall, 1601 E. Market St., Greensboro, NC 27411.
E-mail: ylin@ncat.edu

DOI: 10.1175/WAF-D-14-00080.1

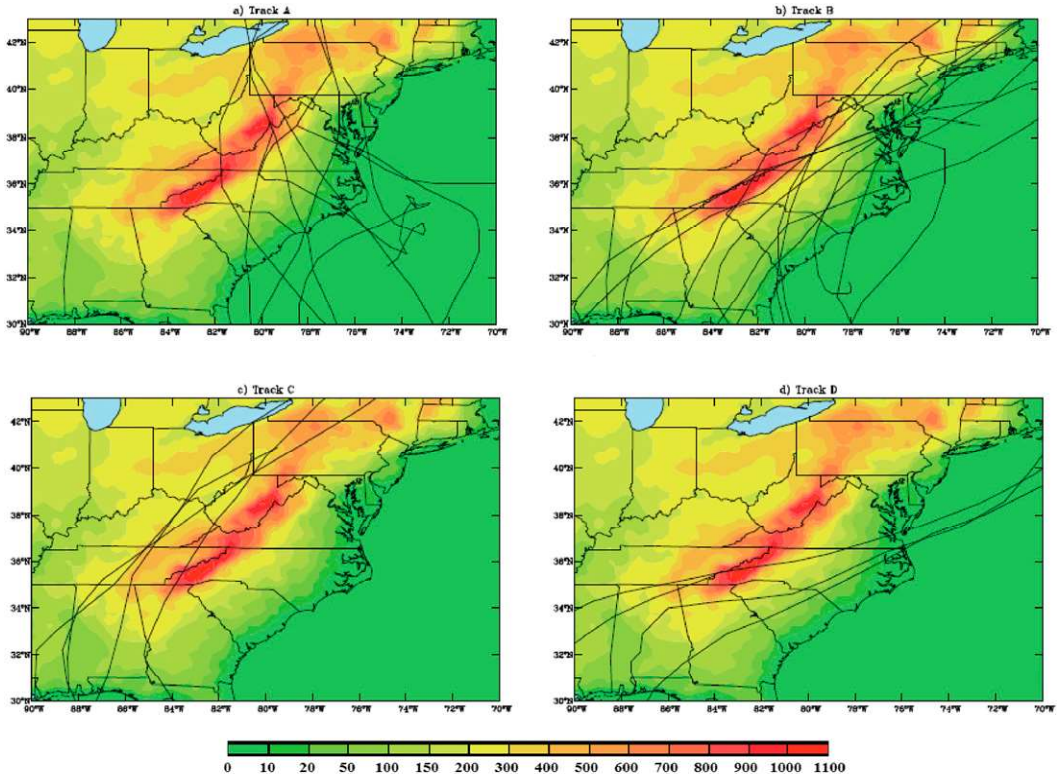

FIG. 1. Track categories (a) A, (b) B, (c) C, and (d) D with topography (m MSL; shaded) proposed by Harville (2009).

the prediction of TCs passing over a mesoscale mountain range, it is vital to understand the dynamics of the TC track continuity and deflection.

Approximately 3200 km long and up to 480 km wide, the Appalachian Mountains extend from eastern Canada to central Alabama and feature ridges, valleys, and plateaus. They are oriented from southwest to northeast with the highest peak of 2037 m at Mount Mitchell, North Carolina. During the hurricane season, from 1 June to 30 November between 1950 and 2001, there was on average one tropical cyclone per year that crossed over the Appalachians (Hart and Evans 2001). A significant number of TCs passing over the northeastern United States pass over the Appalachians. Harville (2009) classified the TC tracks over the Appalachians into four types (Fig. 1): (i) type A, approximately perpendicular to the mountains from east to west; (ii) type B, parallel to the eastern side of the mountains; (iii) type C, parallel to the western side of the mountains; and (iv) type D, similar to type A, but from west to east. In this study, we investigate all TCs passing over the mountains from the east, including type A, and all TCs from the west including type D, regardless of whether they are perpendicular to the mountains or not.

The orographic influence on track continuity and deflection for TCs passing over mountain ranges, such as Taiwan's CMR, has been extensively studied. According to Wang (1980), TCs crossing the CMR had either a continuous or a discontinuous track. Typhoons with discontinuous tracks are normally defined as having two or more secondary low-level pressure centers that form over the lee side of the CMR when the parent cyclone is approaching (Chang 1982; Lin et al. 1999; Wang 1980; Wu and Kuo 1999). In this study, since both tropical cyclones and extratropical cyclones (ETCs) are being considered, the above definition seems to be too strict; thus, a discontinuous track is redefined as a cyclone whose mean sea level pressure (MSLP) center disappears over a mountain range for 6–12 h, only to reappear on the lee side. When the mid- to upper-tropospheric cyclonic circulation associated with the cyclone passes over the mountain and is in phase with one of the secondary vortices that developed within a lee trough, the surface vortex can develop further into a TC (Chang 1982; Wang 1980). In this study, we are interested in exploring the track deflection and discontinuity for TCs passing over the Appalachians that have a different geometry from the CMR.

Track discontinuity may occur as a result of the orographic blocking on the cyclone. When a westward-moving cyclone approaches a mountain, the topography affects the cyclone's basic-flow speed U and maximum

wind speed of the TC vortex V_{max}, causing it to deflect either northward or southward. When the blocking is very strong, a lee cyclone may form and develop further to replace the parent cyclone when the upper-level cyclone passes over the mountain. This will result in a discontinuous track (L05; Lin 2007). L05 proposed a conceptual model with three different regimes for a cyclone vortex passing over a mesoscale mountain range: (i) weak blocking, when the cyclone is slightly deflected northward upstream of the mountain range with continuous track; (ii) moderate blocking, when the cyclone is deflected northward upstream of the mountain range and the secondary vortex forms to the southwest of the mountain range; and (iii) strong blocking, when the cyclone is deflected southward and the secondary cyclone is located to the northwest of the mountain range. The conceptual model proposed by L05 is explained by the local vorticity tendency, which is dominated by the vorticity advection and vorticity stretching while the cyclone is crossing over a mesoscale mountain range [Lin et al. (1999); L05; see Lin and Savage (2011) for a detailed vorticity budget analysis]. Note that the term blocking in this study refers to ''orographic blocking'' and not to the term blocking normally used in synoptic meteorology.

Based on previous idealized and real-case numerical simulations and observational analyses of typhoons passing over Taiwan's CMR, L05 demonstrated that track deflection and continuity are controlled by several major nondimensional parameters. These include the basic-flow Froude number (U/Nh), vortex Froude number (V_{max}/Nh), basic-flow Rossby number (U/fL_x), vortex (Lagrangian) Rossby number (V_{max}/fR), and mountain steepness (h/a). Here, U is the speed of the basic or steering flow perpendicular to the mountain ridge, V_{max} is the maximum wind speed of the TC vortex, N is the Brunt–Väisälä frequency, R is the radius of V_{max}, f is the Coriolis parameter, L_x is the mountain scale in the x direction or facing downstream of the basic flow, h is the mountain height, and a is the horizontal scale of the mountain in the basic-flow direction. Detailed descriptions of these nondimensional control parameters can be found in L05 (see their Fig. 2) and in Lin (2007). L05 concluded that a cyclone experiences less (more) deflection and its track becomes continuous (discontinuous) with a combination of larger (smaller) values of V_{max}/Nh, V_{max}/fR, U/Nh, and U/fL_x, and smaller (larger) values of h/L_x. In addition, they found that track continuity is mainly controlled by V_{max}/Nh and is less sensitive to other parameters, such as V_{max}/fR, U/Nh, and U/fL_x. Although V_{max}/fR was not included as a control parameter for TC track discontinuity in L05, a close look at their Fig. 3b shows that $V_{max}/fR < 4.0$ may be used as a criterion for track discontinuity (except with case 14). As a result, we propose to examine whether V_{max}/fR can be used as another controlling parameter for discontinuity, in addition to V_{max}/Nh. Even though these control parameters have enhanced our understanding of the dynamics of track deflection and discontinuity, it is not clear whether they are applicable to other mountain ranges with differences in size and topography.

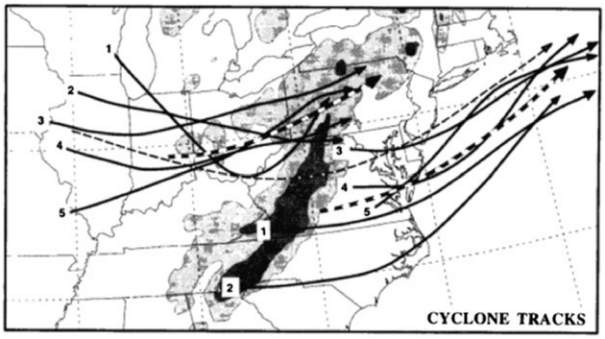

FIG. 2. Five representative ETCs that exhibited redevelopment across the Appalachians (solid lines; O'Handley and Bosart 1996). The heavy dashed lines represent an approximated mean of all primary and secondary cyclones. The thin dashed line denotes an interpolated mean track of the primary cyclones without the orography effect. The shaded areas denote the smoothed topographical contours of 300 and 600 m MSL.

In this study, we hypothesize that the track discontinuity of TCs over the Appalachians is controlled by smaller V_{max}/Nh and V_{max}/fR and is less sensitive to other parameters. Because of the fact that the Appalachians are a lower-elevation mountain range, compared to Taiwan's CMR, the storm tracks should be more continuous. This hypothesis will be tested by estimating and comparing the relative magnitudes of V_{max}/Nh, V_{max}/fR, U/Nh, and U/fL_x based on observed TCs passing over the Appalachians. This will help us determine whether a threshold of track discontinuity, such as $V_{max}/Nh = 1.5$ and $V_{max}/fR = 4.0$ as found in L05, is applicable to the Appalachian cases.

In addition to TCs, O'Handley and Bosart (1996) found that among the ETCs that produced snowstorms in winter and approached the Appalachians from the west or southwest, 70% featured a primary cyclone west of the mountains accompanied by a new secondary cyclone that developed concurrently on the lee side. Approximately 79% of these secondary cyclones redeveloped further into major cyclones over the Atlantic Ocean (Fig. 2). Kocin and Uccellini (2004a,b; hereafter KU04a,b) also found that approximately 50% of the heaviest snowstorms affecting the northeastern urban corridor between the years 1950 and 2003 are also

accompanied by the redevelopment of a secondary cyclone near or along the coastline as soon as the storm was west of the Appalachians. Additionally, the 500-hPa vorticity maximum moved continuously toward the East Coast. Following L05, we hypothesize that stronger blocking associated with the weaker near-surface tangential winds of extratropical cyclones tends to make their tracks discontinuous across the Appalachians. This hypothesis will be tested by investigating 13 extratropical cyclones, which produced heavy snowstorms during the period 1950–2003 and whose tracks are all discontinuous. Note that the reformation of a low on the lee side of a mesoscale mountain range, such as the Appalachians, Rockies, or Alps, may develop into a lee cyclone during the passage of an extratropical cyclone. Based on classical lee cyclogenesis theories, this type of lee cyclogenesis may be explained by vorticity stretching associated with the earth's rotation ($f\partial w/\partial z$), where w, z, and ζ are the vertical velocity, height, and vertical vorticity, respectively, or a preexisting vorticity ($\zeta\partial w/\partial z$) [e.g., see reviews in Pierrehumbert (1986), Smith (1979), and Lin (2007)]. The Weather Research and Forecasting (WRF) Model (Skamarock et al. 2008) tested this hypothesis with a simulation of the 2–5 February 1995 snowstorm.

This paper is organized as follows. Section 2 will feature climatology of the hurricane cases and test the hypothesis that the lack of track discontinuity for TCs passing over the Appalachians is mainly due to larger V_{max}/Nh and V_{max}/fR while being less sensitive to U/Nh and U/fL_x. In section 3, we will test the second hypothesis on track discontinuity of ETCs passing over the Appalachians using cases studied by KU04a,b. Section 4 will include the simulation of a discontinuous track case using the WRF Model as well as an investigation of the aforementioned control parameters. The summary and conclusions can be found in section 5.

2. Climatology for TC track continuity over the south-central Appalachians

All of the TCs from 1851 to 2011 that have impinged on the south-central Appalachians from both the east and west sides of the mountains as explained in the introduction (types A and D) are examined using the Atlantic hurricane database (HURDAT). Among them, 34 TCs belonged to type A and 8 belonged to type D. We are particularly interested in the fact that all of their tracks are continuous. Track details of 16 selected type A and all 8 type D cases can be found in Figs. 3 and 4, respectively.

Based on our hypothesis, track discontinuity is dominated by smaller V_{max}/Nh and V_{max}/fR values while being less sensitive to U/Nh and U/fL_x. To test this hypothesis, V_{max}/Nh, V_{max}/fR, U/Nh, and U/fL_x are calculated (Table 1). For simplicity, we used average values of $h = \sim 1.2$ km, $L_x = \sim 480$ km, $f = \sim 0.84 \times 10^{-4}\,s^{-1}$, and $N = \sim 0.01\,s^{-1}$ (Tables 1 and 2). HURDAT is used to calculate the basic wind speed, which is used to approximate the storm's propagation, V_{max}, and R (the radius of V_{max}). Note that wind radii data for R are available in HURDAT starting at 2004, so R for Hugo (1989) and Isabel (2003) are from our simulated data. The perpendicular component of the basic-flow speed of the storm is used for the calculation of the control parameters. Special care is taken to ensure that both speeds are recorded at a time when the storm had fully developed but had not yet encountered the mountainous Appalachian topography. We accomplished this by drawing a line along the western (eastern) border of the Appalachians and another line parallel and 200 km to the northwest (northeast). This removed the possibility of any appreciable effects between the storm circulation and mountain topography as the eyewall and the significant portion of outer circulation are located within a 200-km radius.

The values for V_{max}/Nh, U/Nh, V_{max}/fR, and U/fL_x are plotted in Fig. 5. The year-to-year variations of U/Nh and V_{max}/Nh are shown in Figs. 5a and 5b, respectively, while the relationship of U/Nh versus V_{max}/Nh is shown in Fig. 5c and U/fL_x and V_{max}/fR versus V_{max}/Nh are shown in Figs. 5d and 5e, respectively. Figures 5b, 5c, 5d, and 5e indicate that V_{max}/Nh is greater than 1.5 for all cases. Note that for stratified fluid flow, a Froude number is considered to be large when it is greater than 1.12. This is because the flow belongs to the regime of flow over a mountain [Miles and Huppert (1969) and Lin and Wang (1996); see Lin (2007) for a brief review]. These results are consistent with our hypothesis because all cases have continuous tracks (Figs. 3 and 4) even though the topographic features, such as the height, steepness, and size of the Appalachians, are completely different from those of the CMR. In particular, the threshold for track continuity, $V_{max}/Nh > 1.5$, coincides with the findings of L05 for TCs passing over Taiwan's CMR. In Fig. 5e, all V_{max}/fR values are above 4.0 for the four continuous TC cases, with the exception of Arlene (2005). This result is also consistent with Fig. 3b in L05 if case 14 out of the 5 cases with continuous tracks is neglected, although it was not stated in their conclusion. Note that U/fL_x varies from 0.03 to 0.38 in Fig. 5d, while U/Nh varies from 0.05 to 0.9 in Figs. 5a and 5c, indicating that track continuity is neither sensitive to U/Nh nor U/fL_x.

In summary, based on Table 1 and Fig. 5, all vortex Froude numbers estimated from the 1851–2011 hurricane tracks give $V_{max}/Nh > 1.5$ and the vortex Rossby number estimated for a limited number of TC cases whenever the data of R was available gives $V_{max}/fR > 4.0$. Thus, the

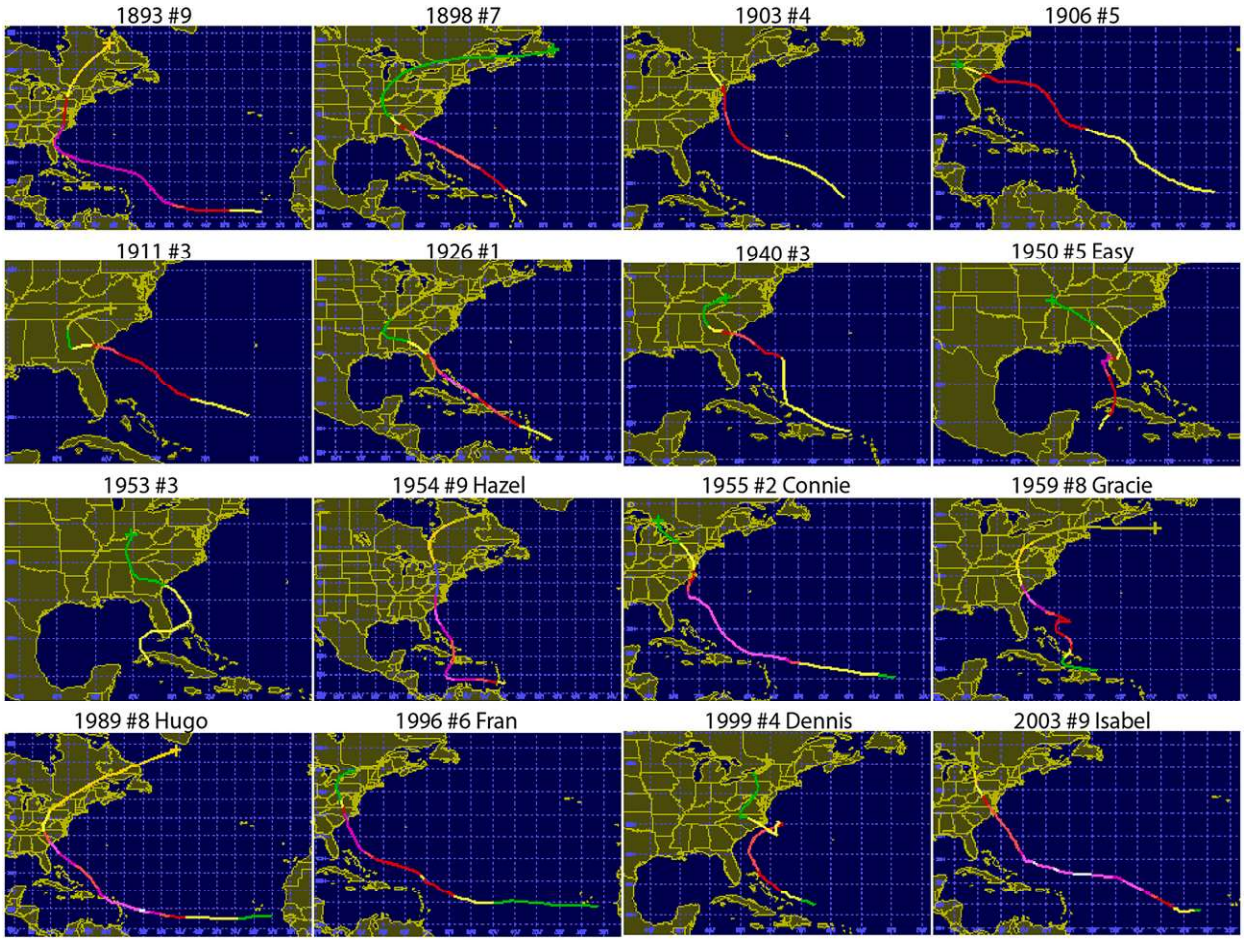

FIG. 3. Sixteen selected tracks of TCs impinging on the Appalachians from the east (denoted as type A) for the period 1851–2010 from HURDAT.

above numbers support the hypothesis proposed earlier since all 1851–2011 hurricane tracks are continuous. This result will be further confirmed in sections 3 and 4 for ETC cases. Note that the nondimensional steepness control parameter (h/L_x) has a small value (~0.0038), indicating that blocking is weak for all cases of types A and D. Figure 5 indicates that cyclone track continuity is controlled by V_{max}/Nh and V_{max}/fR. Furthermore, we also found that track continuity is less sensitive to the basic-flow Froude number (U/Nh) and the basic-flow Rossby number (U/fL_x) (Figs. 5a,c,d).

3. Application of track control parameters of TCs to extratropical cyclones

Approximately 70% of ETCs exhibited a discontinuous track over the Appalachians (O'Handley and Bosart 1996) and 39% of the heaviest snowstorms from 1950 to 2003 experienced redevelopment paths (KU04a,b). A redevelopment path is defined as the path or track of the storm redeveloped from the lee side. Since none of the TC cases displayed discontinuity and there are many discontinuous cases with midlatitude cyclones, the above study is extended to include ETCs as well. Based on L05 and section 2, we hypothesize that stronger blocking associated with weaker near-surface tangential winds of extratropical cyclones tends to make their tracks across the Appalachians discontinuous. We hypothesize further that track continuity is mainly controlled by V_{max}/Nh and V_{max}/fR, while being less sensitive to U/Nh and U/fL_x. This hypothesis will be tested by estimating the nondimensional control parameters V_{max}/Nh, V_{max}/fR, U/Nh, and U/fL_x of past ETC events documented in KU04a,b and in a real-case numerical simulation.

Given the lack of raw data for ETCs and their tracks, we decided to use data from KU04a,b to calculate the control parameters and test our hypotheses. KU04a,b investigated the 30 heaviest snowstorms affecting the NE urban corridor, out of 115 of the most widespread and

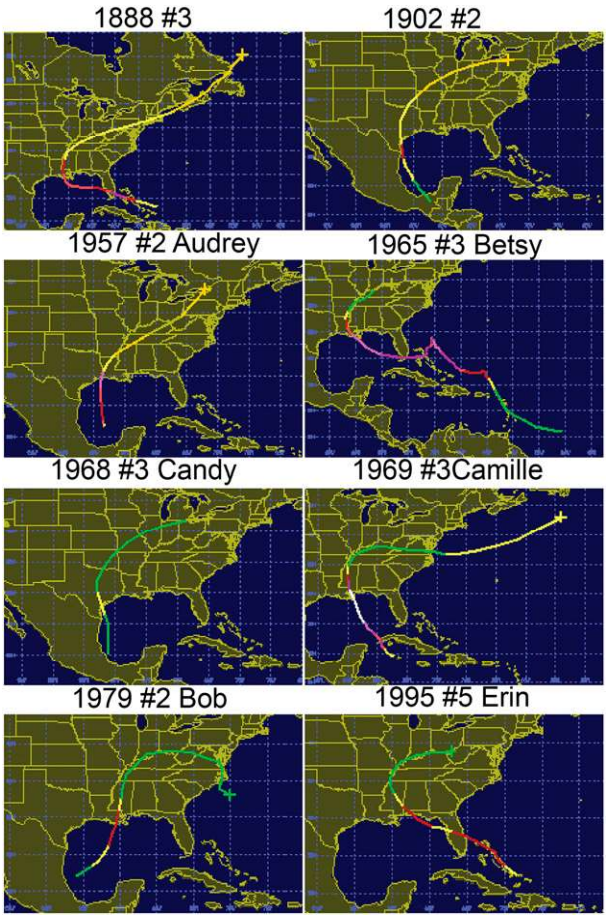

FIG. 4. All eight tracks of TCs impinging on the Appalachians from the west (denoted as type D) for the period 1851–2010 from HURDAT.

significant snowstorm events from 1950 to 2003. Out of these 30 snowstorms, 13 experienced track discontinuity and are categorized as "Atlantic redevelopment paths" by KU04a,b (Fig. 6). They are similar to the type B cyclones of Miller (1946). After performing our own categorization of track types (Fig. 1), no ETCs of type A are found since all of the storms approached the Appalachians from the west. Additionally, none of the type D storms are continuous. From the 13 discontinuous cases, 8 satisfied our type D definition and are chosen for our study (Fig. 7). The storm speed is estimated by dividing the distance the storm traveled by the time it took to cover it. As with the TC cases, only the component perpendicular to the Appalachian mountain range is used. For the estimation of V_{max}, two approaches are taken: one using the average of the total wind and the other using the maximum value of the total wind. This is because we need the maximum tangential wind speed of the storm at a location where the storm has not yet encountered the mountain topography.

Since the minimum MSLP varies in different cases, it is difficult to find one value and calculate the maximum wind around it. As mentioned earlier, this value is found by drawing a line along the western (eastern) border of the Appalachians and a parallel line 200 km to the northwest (northeast), thus ensuring that no appreciable effects occur from the mountain topography on the storm's circulation. In addition, because the total wind includes both the tangential wind speed and the storm's moving speed, calculating both values will give a better estimate of the real tangential wind speed. This is done by taking the average at two levels, 1000 hPa and $\sigma = 0.85$ (or, say, the 850-hPa level upstream over the plain area), and allowed us to estimate the vortex Froude number (V_{max}/Nh) and the vortex Rossby number (V_{max}/fR).

The estimated control parameters (for the second approach) are presented in Table 2, which shows that V_{max}/Nh varies from 0.75 to 1.25. In the first approach, where total wind is averaged, the V_{max}/Nh values are even smaller, ranging from 0.63 to 0.92. In other words, for both approaches, the range of V_{max}/Nh falls below $V_{max}/Nh = 1.5$, as proposed in L05, thus verifying our hypothesis. The estimated V_{max}/fR falls below 4.0, the threshold proposed in section 2. On the other hand, U/Nh varies from 0.13 to 0.96, and U/fL_x varies from 0.06 to 0.43, indicating that there is no particular critical value found to distinguish between the continuous and discontinuous track cases. This is also consistent with TC cases and the theory of L05, as is clearly shown in Fig. 8. Therefore, the theory of L05 applies to both TC and ETC tracks, and V_{max}/fR and V_{max}/Nh can serve as control parameters for discontinuity for both TC and ETC tracks.

The lack (abundance) of discontinuous tracks for TCs (ETCs) is related to the fact that a TC (ETC) has a warm (cold) core. A warm-core cyclone has its maximum cyclonic winds near the surface because the thermal wind blows in the opposite direction of the tangential wind. The cyclonic wind is then weakened at higher levels as required by the thermal wind relation. In contrast, a cold-core cyclone, such as an ETC, has its tangential wind and thermal wind blowing in the same direction. As a result, the cyclonic tangential wind increases with height. This leads to the strongest winds being on the surface of the TC and gives larger V_{max}/Nh and V_{max}/fR values. Physically, this means that a TC has more kinetic energy and latent heat to overcome the potential energy barrier, that is, the blocking, of the mountain. On the other hand, a weaker basic and tangential wind associated with an ETC near the surface gives smaller values for V_{max}/Nh and V_{max}/fR. This means that the ETC has less energy to overcome the blocking or potential energy barrier associated with the mountain, thus making the track more likely to be discontinuous.

TABLE 1. Perpendicular components of the basic wind speed and the max tangential wind speed from HURDAT for the period 1851–2011 used to estimate the basic-flow Froude number, the vortex Froude number, the basic-flow Rossby number, and the vortex Rossby number for track types A and D.

Year	Date	Name	U (m s^{-1})	V_{max} (m s^{-1})	R (10^3 m)	V_{max}/Nh	V_{max}/fR	U/Nh	U/fL_x
1876	12–19 Sep	—	10.2	33.5	—	2.8	—	0.85	0.38
1878	1–13 Sep	—	7.8	40.2	—	3.4	—	0.65	0.29
1885	10–14 Oct	—	4.2	31.3	—	2.6	—	0.35	0.16
1888	14–24 Aug	—	1.9	48.6	—	4.1	—	0.16	0.07
1893	25 Sep–15 Oct	—	3.3	53.6	—	4.5	—	0.28	0.12
1896	4–12 Jul	—	0.9	41.1	—	3.4	—	0.07	0.03
1896	22–30 Sep	—	4.4	52.0	—	4.3	—	0.36	0.16
1898	25 Sep–6 Oct	—	3.7	56.4	—	4.7	—	0.31	0.14
1901	11–15 Jun	—	4.6	17.9	—	1.5	—	0.38	0.17
1901	2–18 Aug	—	0.6	39.1	—	3.3	—	0.05	0.02
1901	21 Sep–2 Oct	—	2.9	20.7	—	1.7	—	0.24	0.11
1902	21–29 Jun	—	1.1	18.3	—	1.5	—	0.10	0.04
1903	12–17 Sep	—	5.0	39.7	—	3.3	—	0.42	0.19
1906	8–14 Jun	—	2.0	22.4	—	1.9	—	0.16	0.07
1906	3–18 Sep	—	5.5	40.2	—	3.4	—	0.46	0.20
1906	19–30 Sep	—	3.8	51.4	—	4.3	—	0.32	0.14
1911	23–31 Aug	—	3.5	40.2	—	3.4	—	0.29	0.13
1915	31 Aug–6 Sep	—	4.4	40.2	—	3.4	—	0.36	0.16
1926	22–31 Jul	—	2.1	52.0	—	4.3	—	0.17	0.08
1928	6–21 Sep	—	4.6	57.0	—	4.7	—	0.38	0.17
1932	26 Aug–4 Sep	—	4.6	31.3	—	2.6	—	0.39	0.17
1932	18–21 Sep	—	1.6	24.6	—	2.0	—	0.13	0.06
1940	5–15 Aug	—	3.3	37.4	—	3.1	—	0.28	0.12
1950	1–9 Sep	Easy	2.2	50.9	—	4.2	—	0.19	0.08
1953	29 Aug–3 Sep	—	3.4	22.4	—	1.9	—	0.28	0.13
1954	5–18 Oct	Hazel	8.2	58.7	—	4.9	—	0.69	0.31
1955	3–15 Aug	Connie	3.0	41.9	—	3.5	—	0.25	0.11
1957	25–29 Jun	Audrey	0.9	54.8	—	4.6	—	0.08	0.03
1959	20 Sep–2 Oct	Gracie	3.4	54.2	—	4.5	—	0.28	0.13
1965	27 Aug–13 Sep	Betsy	0.8	56.4	—	4.7	—	0.07	0.03
1968	22–26 Jun	Candy	3.2	23.1	—	1.9	—	0.26	0.12
1969	14–22 Aug	Camille	1.4	84.0	—	7.0	—	0.12	0.05
1970	19–23 Jul	Becky	1.7	29.1	—	2.4	—	0.14	0.06
1979	9–16 Jul	Bob	2.4	31.3	—	2.6	—	0.20	0.09
1989	10–25 Sep	Hugo	6.5	51.4	74	4.3	8.3	0.54	0.24
1994	14–19 Aug	Beryl	0.8	17.9	—	1.5	—	0.07	0.03
1995	31 Jul–6 Aug	Erin	2.5	35.8	—	3.0	—	0.20	0.09
1996	23 Aug–10 Sep	Fran	3.9	51.4	—	4.3	—	0.32	0.14
1999	24 Aug–8 Sep	Dennis	2.2	24.6	—	2.0	—	0.18	0.08
2003	6–20 Sep	Isabel	4.0	47.8	124	4.0	4.6	0.33	0.15
2005	8–14 Jun	Arlene	3.1	20.1	150	1.7	1.6	0.26	0.12
2005	4–13 Jul	Dennis	5.0	47.8	97	4.0	5.9	0.42	0.19

4. A numerical modeling study of an extratropical cyclone passing over the Appalachians

Based on the eight type D discontinuous cases of the 30 heaviest snowstorms from 1950 to 2003 as discussed in KU04a,b, a typical case, the 3–5 February 1995 snowstorm (also referred to as Feb95), has been chosen to help understand the dynamics associated with orographic blocking.

a. Numerical experimental design

Version 3.4 of the WRF Model is adopted for the simulation. The WRF Model is a fully compressible, three-dimensional, nonhydrostatic model that uses terrain-following vertical coordinates. The governing equations of the WRF Model are written in flux form with conserved mass and dry entropy. In this study, the Runge–Kutta third-order time scheme and the third- and fifth-order advection schemes are chosen for the horizontal and vertical integrations, respectively. The simulation domain contains 160 × 120 grid points with a 36-km horizontal grid resolution (Fig. 9a). The vertical grids are stretched from the surface to the top of the model with a total of 28 levels and the lateral boundaries are kept far from the study area. Feb95 is

TABLE 2. Perpendicular components of the basic wind speed and the max tangential wind speed from KU04a,b for the 8 cases impinging from the west (type D) out of the total of the 30 heaviest snowstorms affecting the northeastern United States for the period 1950–2003 are used to estimate the following: the basic-flow and vortex Froude numbers, and the basic-flow and vortex Rossby numbers.

Year	Date	U (m s^{-1})	V_{max} (m s^{-1})	R (10^3 m)	V_{max}/Nh	U/Nh	U/fL_x	V_{max}/fR
1956	18–20 Mar	10.0	13.0	445.0	1.08	0.83	0.37	0.35
1960	10–13 Dec	1.0	13.0	345.0	1.08	0.32	0.14	0.45
1961	2–5 Feb	0.7	14.0	326.0	1.17	0.22	0.10	0.51
1964	11–14 Jan	0.6	13.0	291.5	1.08	0.19	0.09	0.53
1969	8–10 Feb	3.5	16.0	399.9	1.33	0.59	0.26	0.48
1978	5–7 Feb	11.6	12.0	528.0	1.00	0.96	0.43	0.27
1982	5–7 Apr	0.1	15.0	306.4	1.25	0.13	0.06	0.58
1995	3–4 Feb	0.9	16.0	449.3	1.33	0.29	0.13	0.42

initialized by the GFS model data of KU04a,b at 0000 UTC 3 February and integrated to 1800 UTC 5 February with data being output every 3 h. The time interval is 180 s. The following model physics parameterization or representation schemes are chosen for the present simulation:

- Kain–Fritsch cumulus parameterization scheme,
- WRF single-moment 6-class microphysics scheme (WSM6) with graupel,
- Yonsei University (YSU) PBL parameterization scheme,
- Monin–Obukov surface layer scheme,
- RRTM longwave radiation parameterization scheme, and
- Dudhia shortwave radiation parameterization scheme.

Details of the above schemes and their relevant references can be found in the WRF user's manual (Skamarock et al. 2008).

b. Simulation results

1) TRACK DISCONTINUITY THROUGH SURFACE AND UPPER-AIR ANALYSES

The simulated storm is tracked using its minimum MSLP and by marking the center of the closed isobar, as shown in Fig. 9a. Based on the observed surface data from the National Weather Service (Grumm and Michaud 1996) (Fig. 10), Feb95 started when the low pressure of the parent cyclone was observed at 1200 UTC 3 February over the border of Tennessee and Arkansas. The cyclone moved northeastward through Kentucky while intensifying slowly until it reached eastern Kentucky and deepened to 1002 hPa. At 0300 UTC 4 February, while the cyclone was over West Virginia and approaching the Appalachians, a new secondary low started to develop on the lee side of the Appalachians near northeastern South Carolina. This secondary low continued to develop and became a major storm that ultimately merged with the parent storm. The parent cyclone continued to move northeastward to the Virginia coast and deepened quickly to 992 hPa over eastern Maryland. It continued moving along the northeastern coast until it reached eastern Maine at 0000 UTC 5 February with a minimum MSLP of 972 hPa.

Our simulation track starts 6 h earlier than the observed track and 6 h later than that analyzed by KU04a,b. Beginning at 1200 UTC 3 February (Fig. 9b), the simulated track is slightly to the northwest of the tracks observed and analyzed by KU04a,b. Later, the simulated track is very close to the other two tracks. The minimum MSLP of the parent cyclone is also well simulated, showing clearly the discontinuous track across the Appalachians. The minimum geopotential height at the surface (not shown) can also be used to trace hurricane track discontinuity, which is consistent with that identified by the minimum sea level pressure; however, the MSLP is used in our analysis in order to be consistent when comparing tracks in HURDAT and KU04a,b. The parent cyclone appeared to jump to the lee (eastern) side where it continued to move northeastward. The new cyclone's first appearance is not shown clearly in the track plot since the marking of the minimum MSLP closed isobar did not capture the development of the new cyclone. However, it became more pronounced after strengthening near the Virginia coast.

The minimum MSLP fields (Fig. 11) clearly display the new low that developed on the lee side at 0300 UTC 4 February and the two lows that coexisted on both the upstream and lee sides of the Appalachians. The track may therefore be considered discontinuous as defined in L05 and as described in the introduction. The parent cyclone, as represented by the 1002-hPa isobar at 0300 UTC 4 February, stretched from the northwest to southeast of the mountains, indicating that a new cyclone developed in the northern part of South Carolina. Two obvious lows of 998 hPa can be seen in West Virginia and North Carolina 3 h later at 0600 UTC 4 February. In the southeast, the development of the new cyclone on the lee

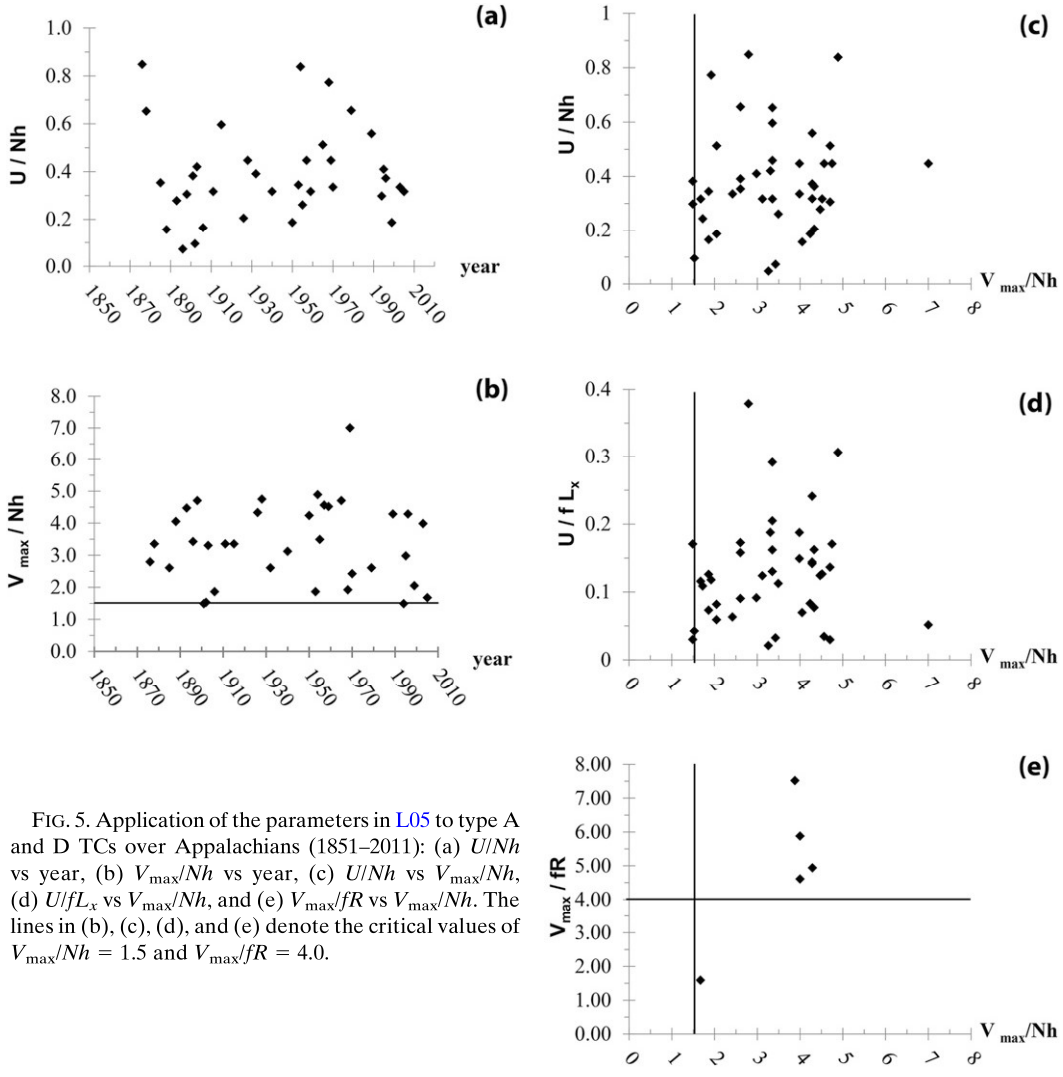

FIG. 5. Application of the parameters in L05 to type A and D TCs over Appalachians (1851–2011): (a) U/Nh vs year, (b) V_{max}/Nh vs year, (c) U/Nh vs V_{max}/Nh, (d) U/fL_x vs V_{max}/Nh, and (e) V_{max}/fR vs V_{max}/Nh. The lines in (b), (c), (d), and (e) denote the critical values of $V_{max}/Nh = 1.5$ and $V_{max}/fR = 4.0$.

side of the mountains can be explained by the positive local vorticity tendency due to vorticity stretching as air descends from the mountains [e.g., Fig. 3.6 of Lin (2007) and relevant discussions]. Similarly, the northeastern movement of the parent cyclone can be explained by the vorticity stretching of the cyclone's outer circulation, which helps the cyclone migrate toward the northwestern corner. Although the earth's rotational effect cannot be ignored in the lee cyclone formation, the relative vorticity stretching plays a more dominant role. This can be proven by performing a budget analysis of the following vorticity equation:

$$\frac{\partial \zeta}{\partial t} = -\mathbf{V}\cdot\nabla\zeta + (\zeta + f)\frac{\partial w}{\partial z} - \left(\frac{\partial w}{\partial x}\frac{\partial v}{\partial z} - \frac{\partial w}{\partial y}\frac{\partial u}{\partial z}\right) - \left(\frac{\partial \alpha}{\partial x}\frac{\partial p}{\partial y} - \frac{\partial \alpha}{\partial y}\frac{\partial p}{\partial x}\right) - \beta v. \quad (1)$$

The vorticity stretching term consists of the stretching through relative vorticity $[\zeta(\partial w/\partial z)]$ and the planetary vorticity $[f(\partial w/\partial z)]$. By comparing these two terms at the lee side where the new cyclone develops, we can determine which mechanism plays a more dominant role on the formation of the new cyclone. From the low-level vorticity (not shown) and from the 500-mb vorticity in Fig. 13 (described in greater detail below), the average relative vorticity on the lee side where the new cyclone developed is $\sim 4 \times 10^{-4}\,s^{-1}$, whereas the range of the planetary vorticity is $\sim 0.854 \times 10^{-4}\,s^{-1}$. This indicates that the stretching through relative vorticity plays a more significant role and thus is the dominant mechanism in lee cyclone development.

The simulated 850-hPa geopotential height and vector wind fields (Fig. 12) are consistent with the results of

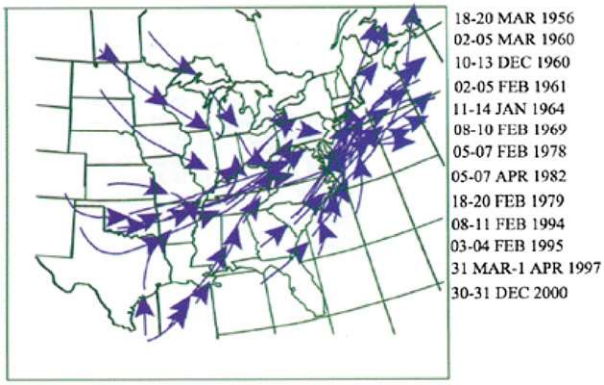

FIG. 6. The discontinuous 13 cases out of the 30 heaviest snowstorms affecting the northeastern United States for the period of 1950–2003 (KU04a,b).

KU04a,b. By 0300 UTC 4 February, the trough over the eastern United States deepened and developed into closed circulation over West Virginia and Ohio, and is associated with a southerly low-level jet of about 20–30 m s^{-1}. The storm then went through a rapid intensification as it moved northeastward along the East Coast with an intensifying low-level jet of 40–50 m s^{-1}. The WRF-simulated 500-hPa geopotential height and vorticity fields (Fig. 13) are also similar to those of KU04a,b. In the early development stage of the storm, there is a deepening trough over central North America with a distinctive vorticity maximum ahead of the trough axis. As the storm reached West Virginia early on 4 February, the trough amplified into a long wave and started to tilt in a negative direction (from southeast to northwest) after passing the Appalachians, consistent with the surface low deepening as it moved northward along the coast. A small disruption in the maximum vorticity occurred at the 500-hPa level while passing over the Appalachians, as can be seen at 0300 and 0600 UTC 4 February (Fig. 13). This disruption occurred during the coexistence of the two surface lows (Fig. 11), indicating that orographic blocking had impacted the 500-hPa flow fields as well. This disruption is not shown in the KU04a,b simulation, which might be due to the long time interval of 12 h.

Similar to tropical cyclones passing over Taiwan's CMR, there is not a significant impact on the 300-hPa flow fields associated with the ETC of Feb95 passing over the Appalachians. This resulted in a continuous track with no disruption (Fig. 14). In addition, the classical negative (northwestward) tilt between the surface cyclone and the upper-level troughs (e.g., 500 and 300 hPa) simulated by the WRF Model (Figs. 11–14) indicated that the environment is favorable for ETC development. The WRF Model is also able to reproduce another important feature, specifically the deepening of the 500- and the 300-hPa troughs over the central United States, a trait common in developing ETCs across the northeast.

It is well known that another major difference between an ETC and a TC is that an ETC strengthens with height in the mid- and upper levels, sometimes exceeding 300 hPa, as a result of the thermal wind balance responding to its cold core. This can also be

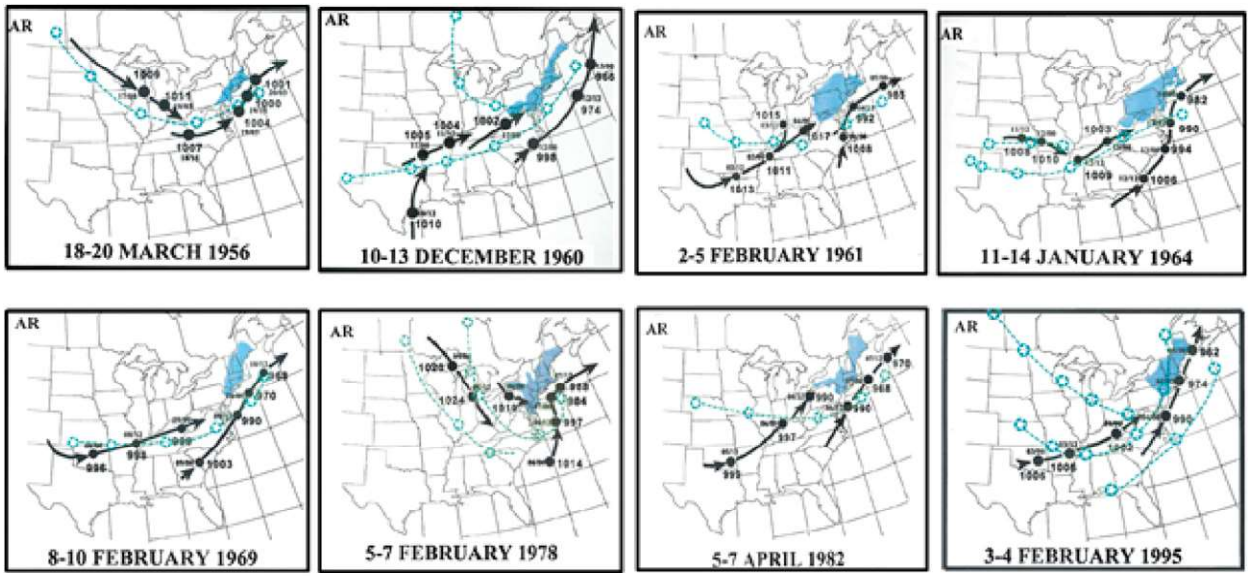

FIG. 7. The selected tracks of the eight cases that belong to both the "Atlantic redevelopment paths" defined by KU04a,b and the type D track defined in this study.

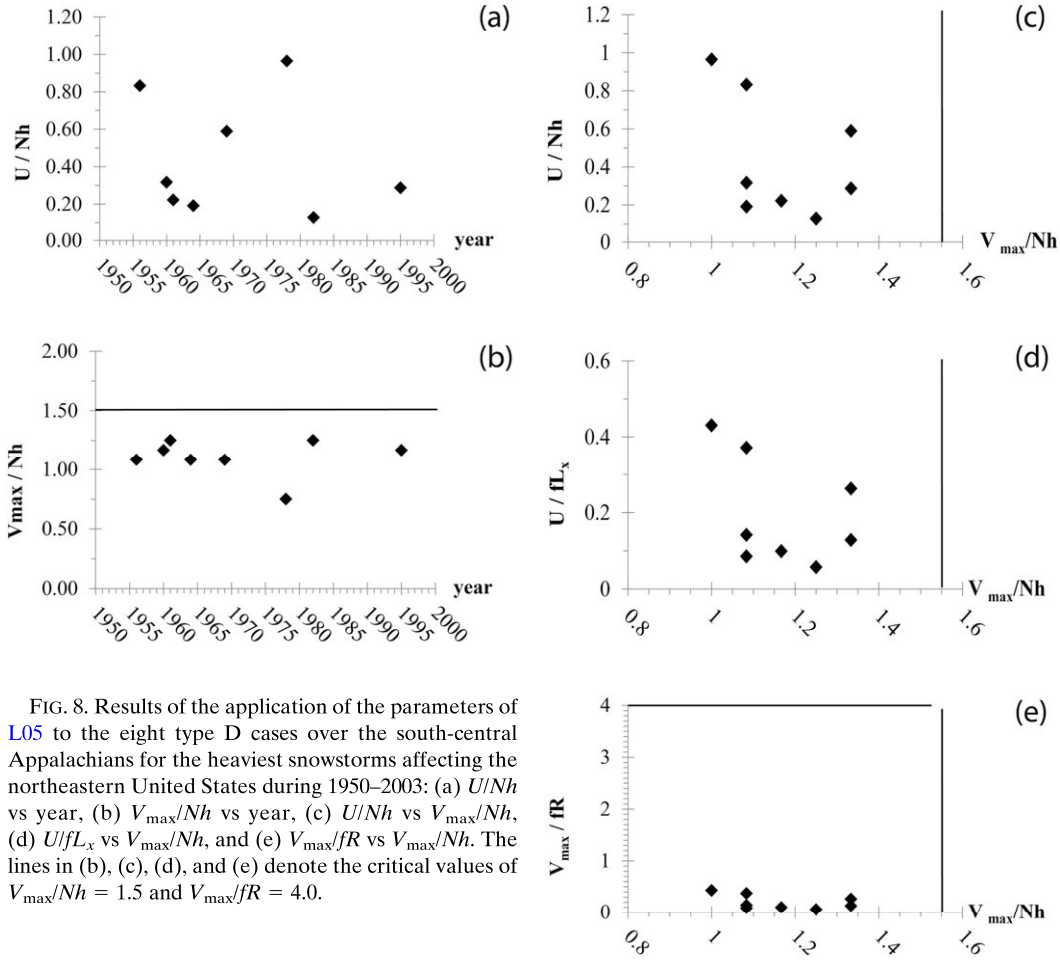

FIG. 8. Results of the application of the parameters of L05 to the eight type D cases over the south-central Appalachians for the heaviest snowstorms affecting the northeastern United States during 1950–2003: (a) U/Nh vs year, (b) V_{max}/Nh vs year, (c) U/Nh vs V_{max}/Nh, (d) U/fL_x vs V_{max}/Nh, and (e) V_{max}/fR vs V_{max}/Nh. The lines in (b), (c), (d), and (e) denote the critical values of $V_{max}/Nh = 1.5$ and $V_{max}/fR = 4.0$.

clearly seen from the 300-hPa total wind speed fields (not shown) in which the wind speed reached higher than $50\,m\,s^{-1}$.

2) CALCULATIONS OF CONTROL PARAMETERS AND OROGRAPHIC EFFECT ON PRECIPITATION

As with the calculation of Froude and Rossby numbers earlier, the storm's moving speed is used as a proxy for the basic wind speed and is estimated by dividing the total distances traveled by time for several time steps. To take into account the effect of moisture, the moist Froude numbers are estimated ($V_{max}/N_w h$ and $U/N_w h$), where $N_w = \sqrt{(g/\theta_v)(\partial\theta_v/\partial z)}$ is the unsaturated Brunt–Väisälä frequency, g is the gravitational acceleration, and θ_v is the virtual potential temperature. We find N_w to be $\sim 0.0115\,s^{-1}$. For two other TC cases (not shown), N_w was estimated and the results came very close to $0.01\,s^{-1}$, making our previously used $N = \sim 0.01\,s^{-1}$ a reasonable approximation. As a result, the effect of using the moist Froude number in this case did not alter the findings of this study. The basic wind speed is estimated to be $20.30\,m\,s^{-1}$, with the perpendicular component $U = 5.25\,m\,s^{-1}$, thereby giving $U/N_w h = 0.38$ and $U/fL_x = 0.2$. For the calculation of V_{max}, we chose 1500 UTC 3 February as the time before the storm encountered the orography. At this time the storm is not far upstream (to the west) and has developed strong circulation (Fig. 15). As seen in Fig. 15, the closed isobars of 1004 hPa have crossed the line 200 km upstream from the Appalachians without encountered the orography. In the first approach, we averaged the total wind speed at the surface (1000 hPa) and 850 hPa as described before to obtain $V_{max} = 5\,m\,s^{-1}$ at the surface and $V_{max} = 20\,m\,s^{-1}$ at 850 hPa. This resulted in averages of $V_{max} = 12.5\,m\,s^{-1}$ and $V_{max}/N_w h = 0.91$. In the second approach, we averaged the maximum tangential wind speeds at the surface ($V_{max} = 9\,m\,s^{-1}$) and at 850 hPa ($V_{max} = 19.5\,m\,s^{-1}$) to obtain $V_{max} = 14.25\,m\,s^{-1}$ and $V_{max}/N_w h = 1.03$. The estimated radius of V_{max} is 449 km, resulting in $V_{max}/fR = 0.38$. In both approaches, the moist vortex Froude number ($V_{max}/N_w h$) is below the threshold of 1.5. The vortex Rossby number is also

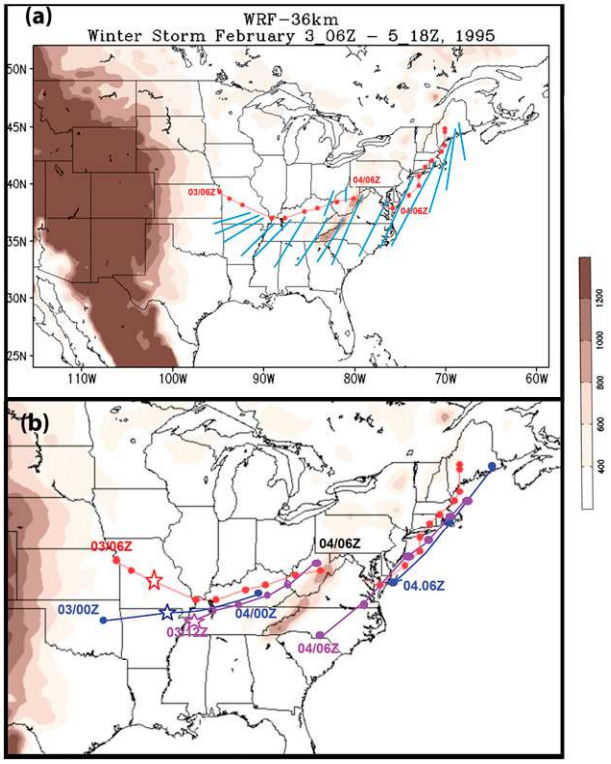

FIG. 9. (a) Simulated storm tracks (dotted in red) from 0600 UTC 3 Feb to 1800 UTC 5 Feb 1995 with min MSLP for every 3 h and local max vorticity strips at 500 hPa (light blue). (b) The WRF-simulated track [red, as in (a)], analyzed track by KU04a,b (blue) from 0000 UTC 3 Feb to 0000 UTC 5 Feb 1995 with data output every 12 h, and the observed track (purple) from 1200 UTC 3 Feb to 0000 UTC 5 Feb 1995 (Grumm and Michaud 1996) for every 3 h. Overlapping red and purple tracks are colored in black. Topography is shaded (m MSL). Same starting time labeled with a star at 1200 UTC 3 Feb 1995.

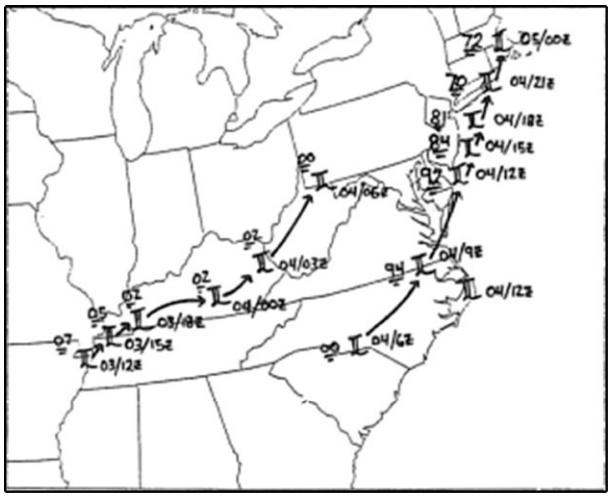

FIG. 10. The cyclone tracks of the 3–5 Feb 1995 TC showing the locations, times, and center surface pressure for observed surface data from the 1200 UTC 3 Feb 1995 forecast cycle (Grumm and Michaud 1996).

below the proposed threshold of 4.0. Thus, from the simulation of this discontinuous ETC associated with a snowstorm passing over the Appalachians and from results of all the discontinuous cases in the previous section, we conclude that a vortex Froude number of 1.5 or less and a vortex Rossby number of 4.0 may also be used for determining the track discontinuity for an ETC passing over a mesoscale mountain. Moreover, we see that the low vortex Froude number and vortex Rossby number can be used to represent the strength of orographic blocking and that the threshold stands for tropical and extratropical cyclones.

Although the main focus of this study is on track discontinuity, it is important to investigate what impact orography has on precipitation, especially when the storm track is discontinuous. Figure 16 shows the potential temperature θ and total precipitation (i.e., rain, snow, and graupel) fields. Precipitation started to form on the windward side when the simulated storm reached the mountains around 0000 UTC 4 February (Fig. 16b) and is later advected to the top of the mountain. Because of the strong downslope winds, the precipitation that is depleted over the downslope appeared to jump to the east (Fig. 16c). This type of jumping behavior is related to the nature of the discontinuous track, which is associated with orographic blocking and lee cyclogenesis. The northern portion of the precipitation is mainly composed of snow (not shown) while over the western side of the mountain it is mainly composed of rain. It appears that the closed circulation at 850 hPa (0300 UTC 4 February) is collocated with heavy precipitation, mainly composed of snow (not shown). Thus, the lack of closed circulation at 850 hPa is also an indication of the lack of heavy precipitation (KU04a,b). The study of the eight discontinuous type D track cases in the previous section indicates that precipitation was mainly composed of snow after the storm passed over the mountains. This is also shown in the snowfall plots of KU04a,b, although the relation between the snow distribution and track discontinuity is not discussed in their storm analysis.

To help understand the dynamics associated with orographic blocking, the equivalent potential temperature θ_e and total water mixing ratio (excluding water vapor) fields from Feb95 are analyzed in a vertical cross section across 37°N (Figs. 17a–d) in order to capture the orographic blocking of the parent cyclone as it passed over the Appalachians. The vertical section across 35°N is used to capture the formation of the new cyclone on the lee side. The very low basic-flow Froude number,

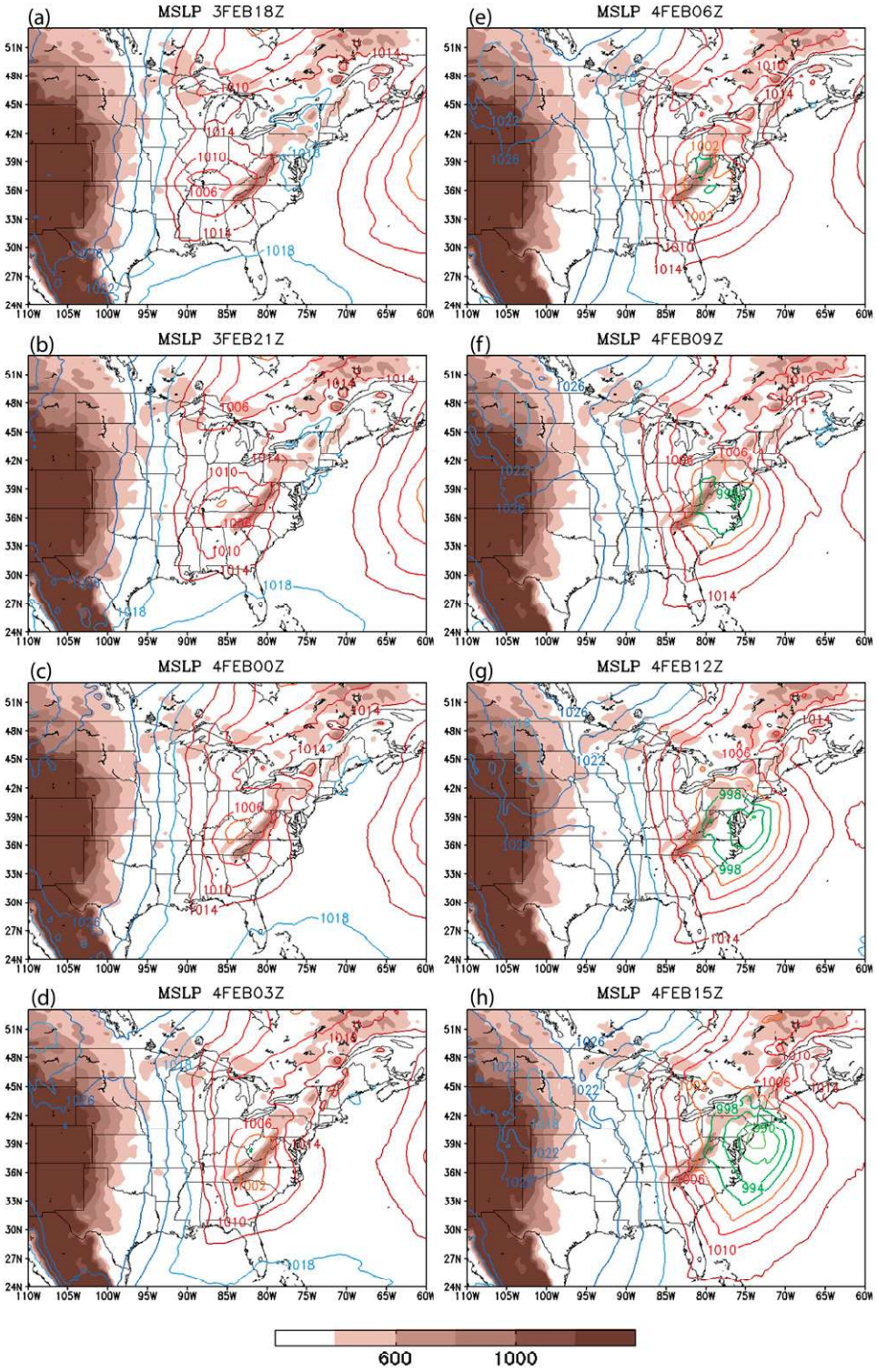

FIG. 11. WRF-simulated MSLP and topography (m MSL; shaded) fields of Feb95: (a) 1800 UTC 3 Feb, (b) 2100 UTC 3 Feb, (c) 0000 UTC 4 Feb, (d) 0300 UTC 4 Feb, (e) 0600 UTC 4 Feb, (f) 0900 UTC 4 Feb, (g) 1200 UTC 4 Feb, and (h) 1500 UTC 4 Feb 1995.

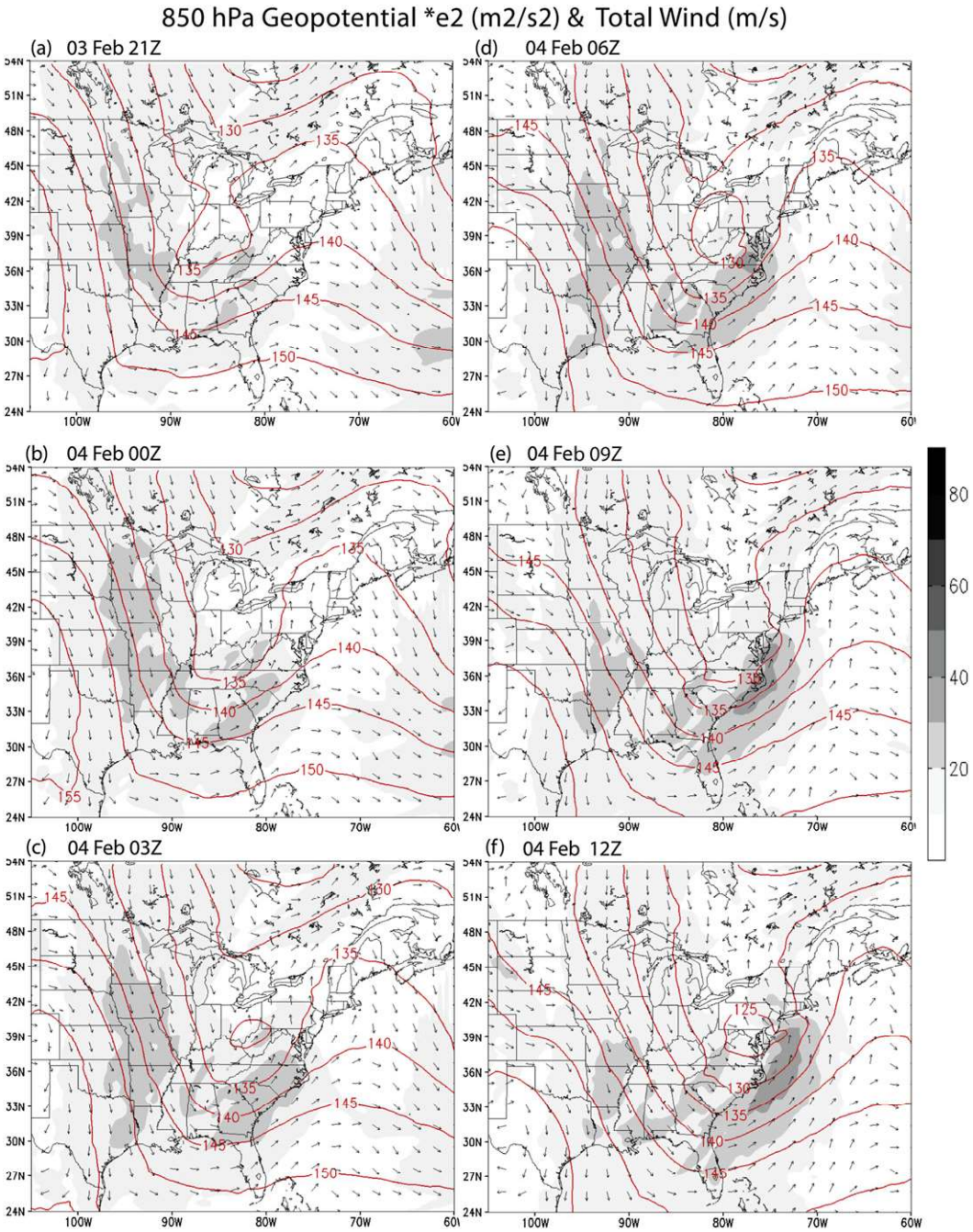

FIG. 12. WRF-simulated 850-hPa geopotential heights (dam; red contours), vector wind, and total wind ($m\,s^{-1}$; shaded) fields of Feb95: (a) 2100 UTC 3 Feb, (b) 0000 UTC 4 Feb, (c) 0300 UTC 4 Feb, (d) 0600 UTC 4 Feb, (e) 0900 UTC 4 Feb, and (f) 1200 UTC 4 Feb 1995.

$U/N_w h = 0.38$, indicates that orographic blocking on the cyclone is very strong. Therefore, this flow pattern belongs to the strong blocking regime, as proposed by L05 [also see Fig. 5.37b of Lin (2007)]. The WRF-simulated θ_e fields indicate strong blocking over the upslope (western slope) of the mountains. This is evident from the θ_e contours, which are almost vertically bent down toward the upslope (e.g., see θ_e = 295, 300, and 305 K in Fig. 17b). Blocking of this kind is well recognized for flow over mountains. Such behavior can be seen in the θ fields [see Fig. 5.10 of Lin (2007)] for a low Froude number flow over a two-dimensional, bell-shaped

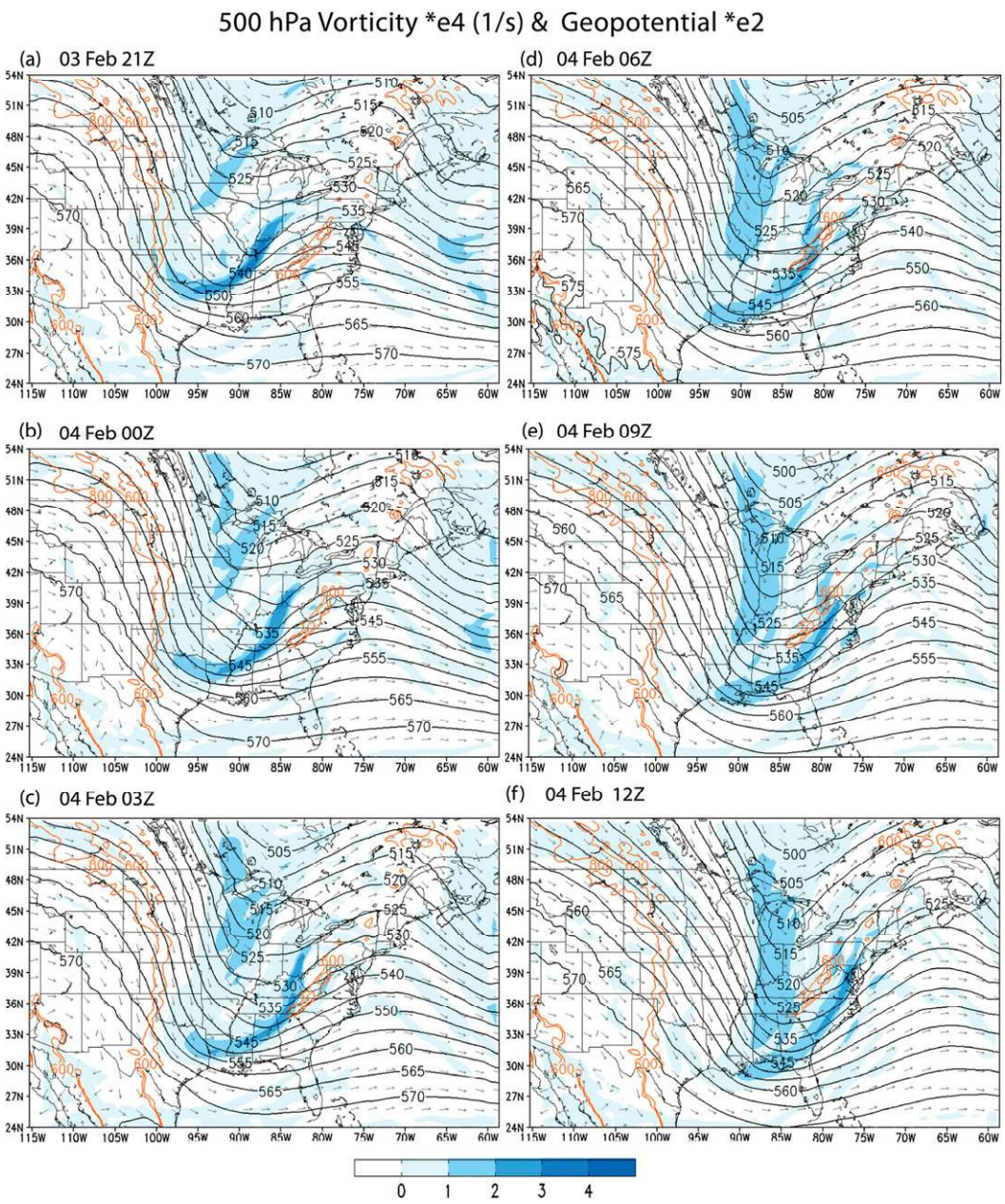

FIG. 13. WRF-simulated 500-hPa geopotential heights (dam; black contours), vector wind, and vorticity (s^{-1}; shaded) fields of Feb95: (a) 2100 UTC 3 Feb, (b) 0000 UTC 4 Feb, (c) 0300 UTC 4 Feb, (d) 0600 UTC 4 Feb, (e) 0900 UTC 4 Feb, and (f) 1200 UTC 4 Feb 1995. Topographical height contours of 600 and 800 m MSL are given (orange).

mountain. Our basic-flow Froude number ($U/N_w h$) of 0.38 fell into the fourth regime of Lin and Wang (1996), where a significant portion of the upstream flow is blocked by the mountain. Along 37°N (Figs. 17a–d), the parent cyclone is captured by the model as it passes over the mountain starting at 2100 UTC 3 February before the mountains strongly affect the cyclone. Prior to the ETC's encounter with the mountains at 0300 UTC 3 February (not shown), the θ_e contours show almost no bending on either side of the mountain. As the storm approaches the mountain at 2100 UTC 3 February, the θ_e contours show blocking on the upstream (western) side and on the eastern slopes. The bending of the θ_e contours on the eastern slopes is in reality the upslope with respect to the outer circulation of the ETC. At the same time, we see the convective clouds that

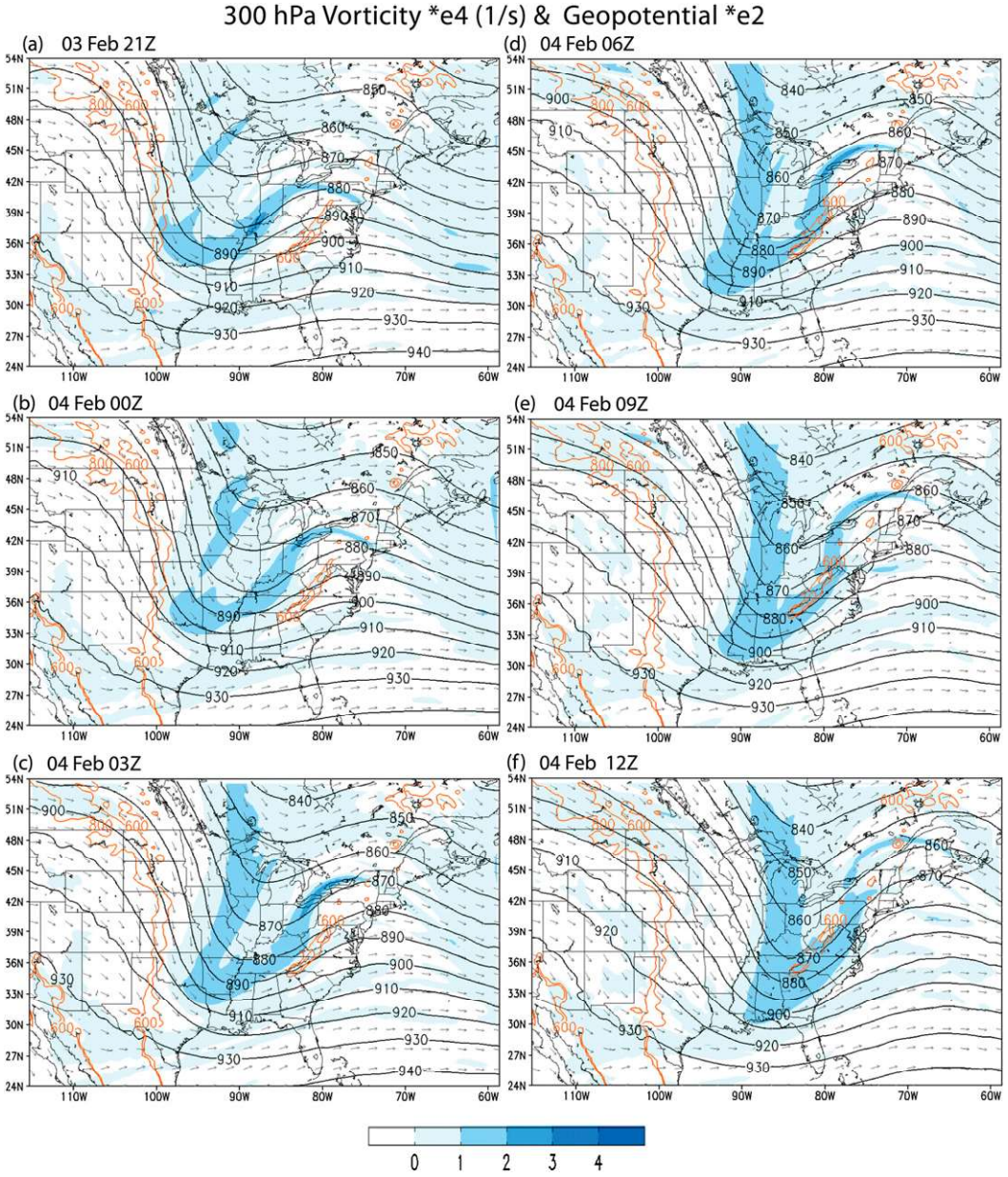

FIG. 14. As in Fig. 13, but for 300 hPa.

accompany the storm approaching the mountains from the west.

As the storm moved eastward at 0000 and 0300 UTC 4 February (Figs. 17b,c), the isentropic (θ_e) contours continue bending down toward the western slopes. We also saw vertical convective cloud formation as the storm passed over the mountains, as well as the cloud mixing ratio contours grouping together. This grouping is indicative of the blocking in the midtroposphere. Some low-level orographic clouds are generated as the storm ascends the upslope on the western side of the mountain. The passage of the storm over the mountain can be detected by observing the strong downward bending of isentropes; first on the western side of the mountain, then the eastern side of the mountain, and finally no bending at all. To capture the new cyclone development, a vertical cross section across 35°N has been analyzed and shown in Figs. 17e and 17f. Only some orographic clouds are present until 0600 UTC 4 February. At this time, we see the low center split and a new cyclone begin to develop (Fig. 17f). The sudden vertical development of clouds on the eastern

side of the mountains is associated with the new cyclone formation on the lee (eastern) side of the Appalachians. At the same time, the parent cyclone moved northeastward on the western side of the mountains across about 37°N (Figs. 17a–d). The new cyclone then redeveloped over the coastal region where it acquired more moisture and heat (Figs. 17e,f).

5. Summary and conclusions

The orographic influence on track continuity for both tropical and extratropical cyclones passing over the south-central Appalachians is examined in this study. In the first portion of this study, it is found that during the period between 1851 and 2011 all 34 TCs passing over the Appalachians from the west (type A) and all 8 TCs from the east (type D) had continuous tracks. Using a hurricane reanalysis dataset (HURDAT), the basic wind speed U and the maximum tangential wind speed V_{max} are used to estimate both the basic-flow and vortex Froude numbers (U/Nh and V_{max}/Nh, respectively) and the basic-flow and vortex Rossby numbers (U/fL_x and V_{max}/fR, respectively) for all type A and D TCs. For each case, both values are chosen at a time when the storm is approaching the mountains but before its outer circulation is significantly affected by the mountains. The normal component of the U velocity perpendicular to the mountain range is then estimated from the approach angle to calculate U/Nh and U/fL_x. For all 42 cases, V_{max}/Nh is found to be greater than 1.5, thus making it a dominant control parameter for TC track continuity compared to U/Nh and U/fL_x. This finding is consistent with L05 for typhoons passing over Taiwan's CMR. It is also found that for some TC cases, V_{max}/fR is greater than 4.0, making it another dominant control parameter for TC track continuity compared to U/Nh and U/fL_x. This is consistent with the results of L05 shown in their Fig. 3b, although it is not stated in their conclusions. When compared to Taiwan's CMR, the physical mechanisms for TC track continuity over the Appalachians is explained by weaker blocking associated with lower mountains.

In the second portion of this study, a climatology analysis is performed to further investigate whether the influence of the basic-flow Froude number, the vortex Froude number, the basic-flow Rossby number, and the vortex Rossby numbers (U/Nh, V_{max}/Nh, U/fL_x, and V_{max}/fR, respectively) on track continuity is applicable to ETCs over the Appalachians. Using data obtained from KU04a,b, 30 of the heaviest snowstorms affecting the northeastern United States from 1950 to 2003 are studied. The basic wind speed is estimated from the distance traveled by the storm between two time steps

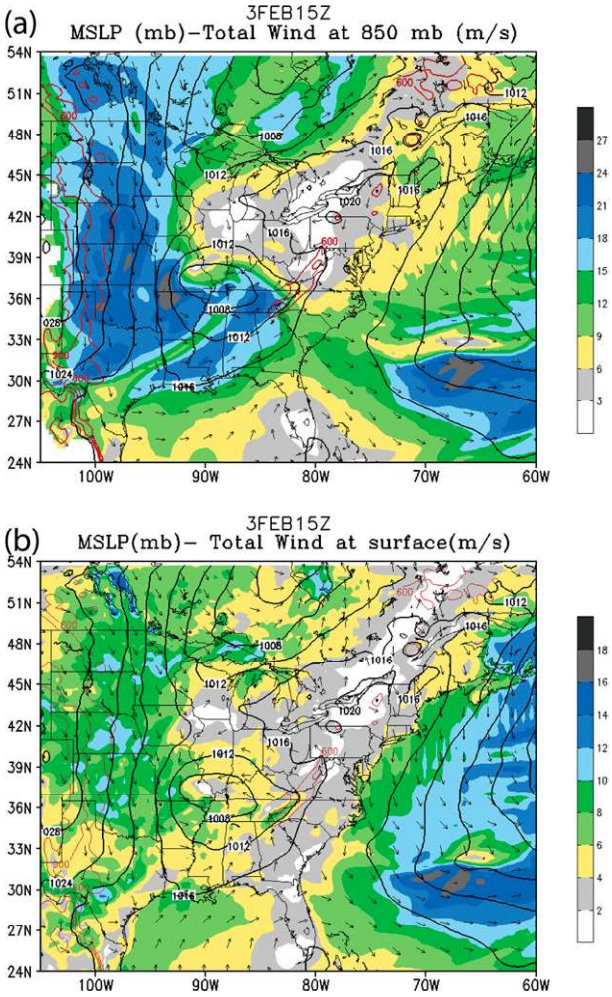

FIG. 15. WRF-simulated total wind fields at (a) 850 and (b) 1000 hPa at 1500 UTC 3 Feb 1995, the same time used to calculate the Froude numbers. The red contours denote the terrain contours of 600 m MSL on average. MSLP fields are contoured in black.

while the normal component to the mountain range is used for estimating the basic-flow Froude number. Two approaches are used in estimating V_{max}. The first is to average the total wind speed and the other is to simply use the maximum value. To ensure accuracy, a layer average between 1000 and 850 hPa is used. The vortex Froude numbers in both approaches are below the 1.5 threshold in all eight discontinuous cases. The vortex Rossby numbers are also below the 4.0 threshold in all eight discontinuous cases. Additionally, it is determined that the basic-flow Froude number and the basic-flow Rossby number play no significant role in track continuity. This finding is consistent with TC cases in the first part of the study as well as that of L05. The dynamics of ETC track continuity are attributed to the weaker

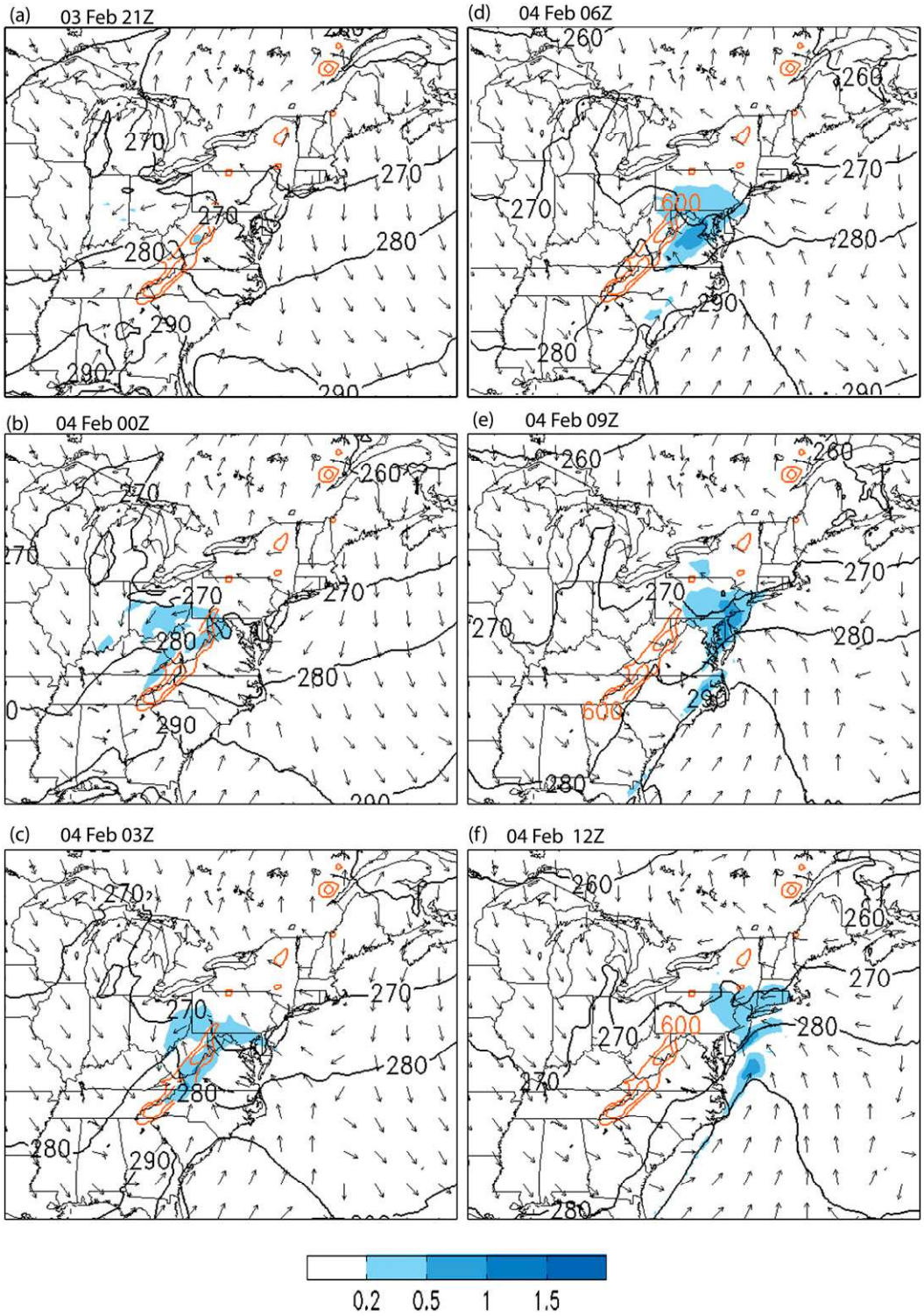

FIG. 16. WRF-simulated precipitation ($g\,kg^{-1}$; shaded) and potential temperature (K) fields of Feb95: (a) 2100 UTC 3 Feb, (b) 0000 UTC 4 Feb, (c) 0300 UTC 4 Feb, (d) 0600 UTC 4 Feb, (e) 0900 UTC 4 Feb, and (f) 1200 UTC 4 Feb 1995. Topographical height contours of 600 and 800 m MSL are given (orange).

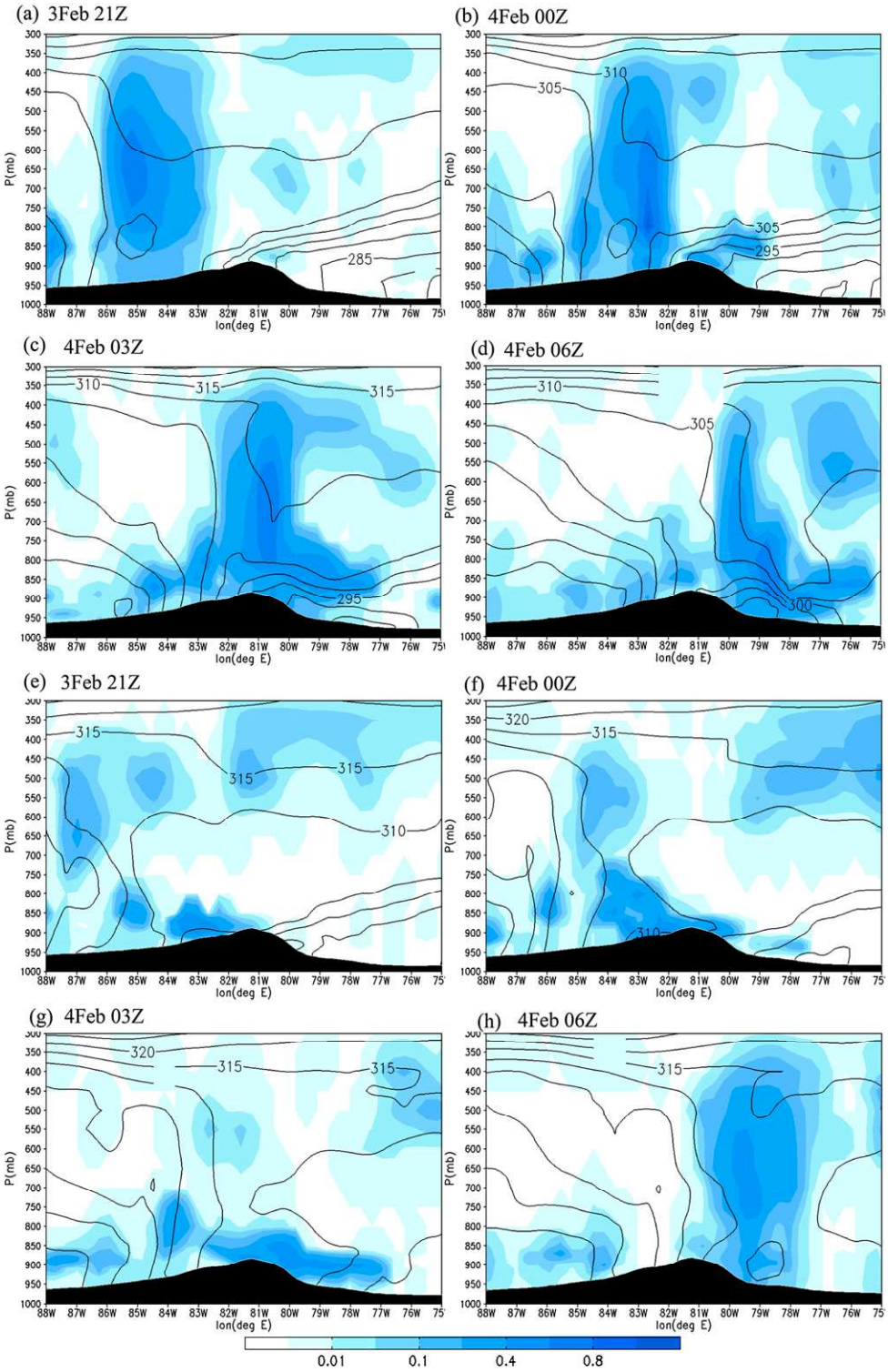

FIG. 17. WRF-simulated vertical cross section of potential temperature and total water content (excluding water vapor) fields across 37°N for (a) 2100 UTC 3 Feb, (b) 0000 UTC 4 Feb, (c) 0300 UTC 4 Feb, and (d) 0600 UTC 4 Feb 1995. (e)–(h) As in (a)–(d), but for across 35°N.

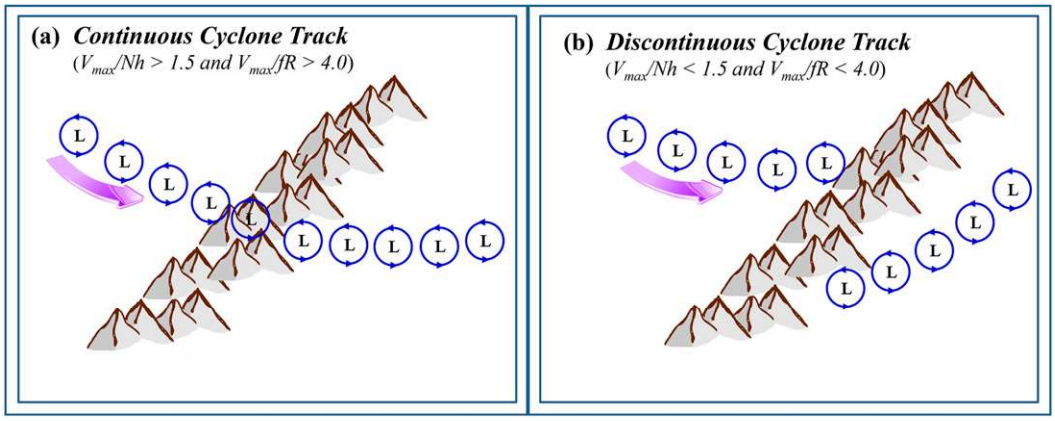

FIG. 18. Schematic model illustrating the mountain range, the TC, and the control parameters for the (a) continuous track passing over the mountain and (b) discontinuous track with the cyclone disappearing and then reappearing on the lee side. The thresholds for the nondimensional parameters have been added for both cases.

near-surface winds that are inherently associated with ETCs, as required by the thermal wind balance with cold-core ETCs.

The third portion of this study is to further test our hypothesis and to help understand the dynamics associated with orographic blocking by performing a numerical simulation of Feb95 with the WRF Model. Our simulated cyclone track and flow fields are consistent with the analysis and observations of KU04a,b. The track is discontinuous as a result of the coexistence of a surface low with the parent cyclone upstream of the Appalachians and a newly developed low on the lee side. The model is able to reproduce the redevelopment of the leeside low into a storm with closed circulation and winds reaching 40–50 m s^{-1} as it moved along the East Coast. The WRF Model reproduced the evolution of deepening troughs at 500 and 300 hPa and a negative (northwestward) tilt after passing the Appalachians, with and without orographic disruption on the 500- and 300-hPa troughs, respectively, and the northwestward tilt of the surface low to the mid- and upper-level trough.

The same methodology mentioned in the second portion of this study is used to obtain the basic-flow wind speed and the maximum tangential wind speed. Moist Froude numbers are estimated in this case to take into account the effect of moisture, but the differences in the results are insignificant compared to the results using dry Froude numbers. Our results ($V_{\max}/N_w h$ = 0.91 and 1.03; $V_{\max}/fR$ = 0.38) confirmed the findings in the first and second portions of this study. Moreover, they are consistent with the results of L05. We conclude that the track discontinuities of both TCs and ETCs, while less sensitive to U/Nh and U/fL_x, are controlled by small values of $V_{\max}/Nh$ and $V_{\max}/fR$ as a result of strong orographic blocking. To summarize the discussion, Fig. 18 is provided as a schematic model to illustrate the mountain range, the cyclone, and the control parameters.

Figure 18a shows the continuous track passing over the mountain and Fig. 18b shows the discontinuous track with the cyclone disappearing and then reappearing on the lee side. The thresholds for the nondimensional parameters have been added for both cases.

The results from the potential temperature and precipitation fields showed that precipitation on the windward side is advected to the top of the mountain and appeared to quickly move eastward due to the depletion of precipitation associated with adiabatic warming produced by the downslope wind. As found in the analysis of KU04a,b, the lack of heavy precipitation before the storm passed the Appalachians is due to a lack of closed circulation at 850 hPa. The passing of Feb95's parent cyclone is detected by the simulated strong bending of the isentropes and the vertical convective cloud development due to strong orographic blocking. Another cross section at 35°N is completed to capture the new lee cyclone development. It is marked by the sudden vertical cloud development on the eastern side of the mountains. The impacts of orography on the precipitation system associated with the snowstorm and its relationship with track discontinuity are of vital importance and deserve a separate, more thorough study.

Acknowledgments. The comments made by Drs. L. Liu, A. Mekonnen, Y. Rastigejev, and J. Zhang, as well as three anonymous reviewers, are highly appreciated, and have improved the quality of the paper significantly. The authors thank Michelle Lin, Richard

Allen, and Guy Oldaker for proofreading the manuscript. This research was supported by National Science Foundation Awards AGS-1265783, HRD-1036563, OCI-1126543, and CNS-1429464. RR would also like to acknowledge the support from the National Oceanic and Atmospheric Administration Educational Partnership Program under Cooperative Agreement NA06OAR4810187 (2006-2012) in the beginning of her Ph.D. study.

REFERENCES

Atallah, E. H., and L. F. Bosart, 2003: The extratropical transition and precipitation distribution of Hurricane Floyd (1999). *Mon. Wea. Rev.*, **131**, 1063–1081, doi:10.1175/1520-0493(2003)131<1063:TETAPD>2.0.CO;2.

——, ——, and A. Aiyyer, 2007: Precipitation distribution associated with landfalling tropical cyclones over the eastern United States. *Mon. Wea. Rev.*, **135**, 2185–2206, doi:10.1175/MWR3382.1.

Chang, S. W.-J., 1982: The orographic effects induced by an island mountain range on propagating tropical cyclones. *Mon. Wea. Rev.*, **110**, 1255–1270, doi:10.1175/1520-0493(1982)110<1255:TOEIBA>2.0.CO;2.

Franklin, J. L., and Coauthors, 2006: Atlantic hurricane season of 2004. *Mon. Wea. Rev.*, **134**, 981–1025, doi:10.1175/MWR3096.1.

Grumm, R. H., and D. L. Michaud, 1996: East Coast winter storm: 4 February 1995. *Natl. Wea. Dig.*, **20** (4), 13–25.

Hart, R. E., and J. L. Evans, 2001: A climatology of the extratropical transition of Atlantic tropical cyclones. *J. Climate*, **14**, 546–564, doi:10.1175/1520-0442(2001)014<0546:ACOTET>2.0.CO;2.

Harville, S. L., 2009: Effects of Appalachian topography on precipitation from landfalling hurricanes. M.S. thesis, Dept. of Marine, Earth, and Atmospheric Sciences, North Carolina State University, 320 pp. [Available online at http://repository.lib.ncsu.edu/ir/handle/1840.16/2849.]

Kocin, P. J., and L. W. Uccellini, 2004a: *Overview*. Vol. 1. *Northeast Snowstorms*. *Meteor. Monogr.*, No. 52, Amer. Meteor. Soc., 296 pp.

——, and ——, 2004b: *The Cases*. Vol. 2. *Northeast Snowstorms*. *Meteor. Monogr.*, No. 52, Amer. Meteor. Soc., 524 pp.

Lin, Y.-L., 2007: *Mesoscale Dynamics*. Cambridge University Press, 630 pp.

——, and T.-A. Wang, 1996: Flow regimes and transient dynamics of two-dimensional stratified flow over an isolated mountain ridge. *J. Atmos. Sci.*, **53**, 139–158, doi:10.1175/1520-0469(1996)053<0139:FRATDO>2.0.CO;2.

——, and L. C. Savage III, 2011: Effects of landfall location and the approach angle of a cyclone vortex encountering a mesoscale mountain range. *J. Atmos. Sci.*, **68**, 2095–2106, doi:10.1175/2011JAS3720.1.

——, J. Han, D. W. Hamilton, and C.-Y. Huang, 1999: Orographic influence on a drifting cyclone. *J. Atmos. Sci.*, **56**, 534–562, doi:10.1175/1520-0469(1999)056<0534:OIOADC>2.0.CO;2.

——, S.-Y. Chen, C. M. Hill, and C.-Y. Huang, 2005: Control parameters for the influence of a mesoscale mountain range on cyclone track continuity and deflection. *J. Atmos. Sci.*, **62**, 1849–1866, doi:10.1175/JAS3439.1.

Miles, J. W., and H. E. Huppert, 1969: Lee waves in a stratified flow. Part 4. Perturbation approximations. *J. Fluid Mech.*, **35**, 497–525, doi:10.1017/S0022112069001248.

Miller, J. E., 1946: Cyclogenesis in the Atlantic coastal region of the United States. *J. Meteor.*, **3**, 31–44, doi:10.1175/1520-0469(1946)003<0031:CITACR>2.0.CO;2.

O'Handley, C., and L. F. Bosart, 1996: The impact of the Appalachian Mountains on cyclonic weather systems. Part I: A climatology. *Mon. Wea. Rev.*, **124**, 1353–1373, doi:10.1175/1520-0493(1996)124<1353:TIOTAM>2.0.CO;2.

Pierrehumbert, R. T., 1986: Lee cyclogenesis. *Mesoscale Meteorology and Forecasting*, P. S. Ray, Ed., Amer. Meteor. Soc., 493–515.

Schwarz, F. K., 1970: The unprecedented rains in Virginia associated with the remnants of Hurricane Camille. *Mon. Wea. Rev.*, **98**, 851–859, doi:10.1175/1520-0493(1970)098<0851:TURIVA>2.3.CO;2.

Skamarock, W. C., and Coauthors, 2008: A description of the Advanced Research WRF version 3. NCAR Tech. Note–475+ STR, 113 pp. [Available online at http://www.mmm.ucar.edu/wrf/users/docs/arw_v3.pdf.]

Smith, R. B., 1979: The influence of mountains on the atmosphere. *Advances in Geophysics*, Vol. 21, Academic Press, 87–230.

Stewart, S., 2005: Hurricane Ivan 2–24 September 2004. National Hurricane Center Tropical Cyclone Rep., 44 pp. [Available online at http://www.nhc.noaa.gov/data/tcr/AL092004_Ivan.pdf.]

Wang, S.-T., 1980: Prediction of the movement and strength of typhoons in Taiwan and its vicinity. National Science Council Res. Rep. 108, Taipei, Taiwan, 100 pp.

Wu, C.-C., and Y.-H. Kuo, 1999: Typhoons affecting Taiwan: Current understanding and future challenges. *Bull. Amer. Meteor. Soc.*, **80**, 67–80, doi:10.1175/1520-0477(1999)080<0067:TATCUA>2.0.CO;2.